Journal of Structural Geology 31 (2009) 3–10

Contents lists available at ScienceDirect

Journal of Structural Geology

journal homepage: www.elsevier.com/locate/jsg

Some new aspects of kinematic vorticity analysis in naturally deformed quartzites

P. Xypolias*

Department of Geology, University of Patras, GR-26500 Patras, Greece

ARTICLE INFO

Article history:
Received 2 March 2008
Received in revised form 8 September 2008
Accepted 30 September 2008
Available online 1 November 2008

Keywords:
Oblique foliation
Quartz *c*-axis-fabric
Finite strain
Vorticity
Quartzite

ABSTRACT

Two vorticity methods have been proposed to estimate kinematic vorticity number in naturally deformed quartzites. These combine the degree of quartz *c*-axis-fabric asymmetry either with the strain-ratio in the *XZ*-plane of finite strain (R_{XZ}) or with the angle, δ, between the oblique-grain-shape fabric and the main foliation. Here, it is suggested that the incorporation of R_{XZ} data with angle δ values can also serve as an additional method of vorticity analysis. The use of a new nomogram that provides a rapid means of evaluating the consistency of vorticity estimates obtained by the three methods is also discussed. A comparison of vorticity estimates from low-grade test samples using all methods yields that three methods may record different parts of deformation history. This hypothesis was then used to discuss the spatial and temporal variation of kinematic vorticity in a crustal-scale shear zone. This natural example showed that the new method is able to record late-stage changes in the flow regime, which are slightly or not detectable by previous methods. Also, it is noteworthy that vertical vorticity profiles based on results of rigid porphyroclast analysis tend to 'average' profiles obtained by the estimates of quartz based methods.

1. Introduction

Over the last two decades a number of methods have been established to quantify shear-induced vorticity in naturally deformed rocks. Porphyroclast systems, crystallographic fabrics, deformed sets of veins and dikes, and the orientation of finite strain with respect to shear zone boundaries (Law et al., 1984; Platt and Behrmann, 1986; Passchier, 1987; Passchier and Urai, 1988; Wallis, 1992; Simpson and De Paor, 1993; Tikoff and Fossen, 1995; Jessup et al., 2007) are some common vorticity criteria used in these methods. Most of the vorticity methods utilize data collected on the *XZ*-plane of the finite strain (parallel to lineation and normal to foliation) and commonly assume steady-state monoclinic flow with the vorticity vector approximately parallel to the *Y*-axis of the strain ellipsoid. Within this frame, the kinematic vorticity number (W_n), which represents a numerical measure of vortical flow, is often defined as the cosine of the acute angle θ between the flow apophyses (Fig. 1a) and ranges from 0 for pure shear to 1 for simple shear (Means et al., 1980; Bobyarchick, 1986; Passchier, 1988).

Although, most of the critical limitations of the vorticity methods can be independently checked, at least in specimen scale (e.g. Srivastava et al., 1995; Jiang and Williams, 1998; Forte and Bailey, 2007; Iacopini et al., 2008), the assumption of steadiness of deformation through time remains a fundamental problem (Passchier and Trouw, 2005). This problem can be encountered by using the quantity W_m that expresses the mean value of W_n over time (Passchier, 1988). For steady-state progressive deformation W_m (finite deformation) is equal to W_n (instantaneous deformation). However, most of the vorticity methods likely record parts of the deformation history (Passchier, 1988; Wallis, 1992; Law et al., 2004) and therefore, may not provide accurate enough estimates of W_m if deformation is non-steady-state. Even so, the application as many vorticity methods as possible in a given sample, it has proved extremely useful in evaluating the mean vorticity of flow and its spatial variation within large scale shear zones (Wallis, 1995; Grasemann et al., 1999; Xypolias and Koukouvelas, 2001; Bailey and Eyster, 2003; Law et al., 2004; Xypolias and Kokkalas, 2006; Jessup et al., 2006; Sullivan, 2008). This study built on previously proposed methods of vorticity analysis in naturally deformed quartzites (Wallis, 1992, 1995) and suggests an additional method for extracting W_n from this rock type. Findings of this study are also used to discuss the spatial and temporal variation of kinematic vorticity in a crustal-scale shear zone.

2. Vorticity analysis in quartzites – previous works

Wallis (1992, 1995) has proposed two techniques for quantifying the vorticity of flow in naturally deformed quartzites: the

* Tel./fax: +30 2610 994485.
E-mail address: p.xypolias@upatras.gr

0191-8141/$ – see front matter © 2008 Elsevier Ltd. All rights reserved.
doi:10.1016/j.jsg.2008.09.009

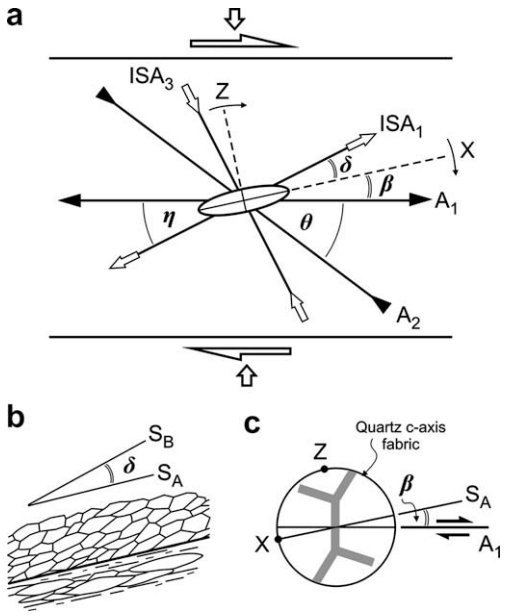

Fig. 1. (a) Simplified sketch showing the relative orientation of instantaneous flow elements and their angular relationships in real space for a dextral general shear flow. A_1 and A_2 – flow apophyses; ISA_1 and ISA_3 – instantaneous stretching axes; X and Z – principal strain axes. The vorticity vector lies perpendicular to the page. (b) The angle, δ, between the oblique-grain-shape fabric (S_B) and the main foliation (S_A) is inferred to be equal to the angle between the ISA_1 and the principal finite strain axis X. (c) The angle, β, between the perpendicular to the central girdle segment of quartz c-axis-fabric and the main foliation (S_A) is inferred to be equal to the angle between the flow apophysis A_1 (flow plane) and the principal finite strain axis X.

oblique-grain-shape/quartz c-axis-fabric method, and the strain-ratio/quartz c-axis-fabric method. These methods are based on two critical assumptions, which are briefly summarized below:

(1) Under progressive simple, pure and general shear, the central girdle segment of quartz c-axis-fabrics develops nearly orthogonal to the flow/shear plane (A_1) (Platt and Behrmann, 1986; Vissers, 1989; Wallis, 1992). This assumption is strongly supported by both experimental (e.g. Bouchez and Duval, 1982; Herwegh and Handy, 1996; Herwegh et al., 1997) and numerical simulation data (e.g. Lister and Hobbs, 1980) as well as by observations in naturally deformed rocks (e.g. Law, 1990; Sullivan and Law, 2007). Therefore, the angle, β, between the perpendicular to the central girdle segment of quartz c-axis-fabric and the foliation (S_A) is equal to the angle between the flow plane (A_1) and the flattening plane of finite strain (Fig. 1a,c; Wallis, 1992). On the base of a recent experimental work (Heilbronner and Tullis, 2006), the above assumption appears not strictly valid in deformed quartzite samples that are characterized by regime-III dynamic recrystallization (Hirth and Tullis, 1992).

(2) The long axes of quartz neoblasts within an oblique-grain-shape foliation (S_B in the sense of Law et al., 1984) align nearly parallel to the extensional instantaneous stretching axis (ISA_1) (Fig. 1a,b; Wallis, 1995). Support for this assumption is given by experimental works which have shown that the oblique foliation (S_B) has a fixed orientation with respect to the external kinematic frame (A_1) during progressive non-coaxial shearing (Ree, 1991; Herwegh et al., 1997; Herwegh and Handy, 1998). This is interpreted to be the result of a complex process of continuous nucleation, passive deformation and rotation of the recrystallized grains composing the S_B (e.g. Means, 1981). Therefore, the maximum observed angle, δ, between the S_B and the main (S_A) foliation is equal to the angle between the ISA_1 and the largest principal axis, X, of the finite strain (Fig. 1a,b; Wallis, 1995).

According to the oblique-grain-shape/quartz c-axis-fabric method (referred to hereinafter as δ/β-method), if both angles δ and β are known then an estimate of vorticity number can be obtained using the equation (Wallis, 1995):

$$W_m = \sin 2\eta = \sin 2(\delta + \beta), \tag{1}$$

where η defines the acute angle between the ISA and the flow apophyses (Fig. 1a; e.g. Weijermars, 1991). Note that Eq. (1) only holds for two-dimensional flow. The δ/β-method is thought to record the last increments of plastic deformation (Wallis, 1995).

The strain-ratio/quartz c-axis-fabric method (referred to hereinafter as R_{XZ}/β-method) is an improvement of the semi-quantitative technique proposed by Platt and Behrmann (1986), and incorporates strain data measured in the XZ-plane of finite strain (R_{XZ}) with the angle β between the flow plane (A_1) and the S_A foliation as determined from quartz c-axis-fabric. Wallis (1992, 1995) demonstrated that for a given pair of values (R_{XZ}, β), the W_m can be estimated either by constructing the Mohr-circle for finite deformation in stretch space or by using the following analytical solutions:

$$\varphi = \tan^{-1}\left\{\frac{\sin 2\beta}{[(R_{XZ}+1)/(R_{XZ}-1)] - \cos 2\beta}\right\} \tag{2}$$

$$W_m = \sin\varphi\frac{R_{XZ}+1}{R_{XZ}-1}. \tag{3}$$

For monoclinic deformation, the R_{XZ}/β-method is equivalent to the R_{XZ}/Θ'-method (Tikoff and Fossen, 1995; Bailey and Eyster, 2003), which utilizes the angle (Θ') between the long axis of the finite strain ellipsoid and the shear zone boundary (A_1) to estimate the W_m. Bailey et al. (2004) argued that this method does not requires the assumption of steady-state deformation. However, vorticity number estimates using R_{XZ}/β-method are very sensitive to small changes in the evaluated angle β (Grasemann et al., 1999; Law et al., 2004; Bailey et al., 2004). Note that in most quartz c-axis-fabric diagrams the angle β can be evaluated with an error $\pm 2^\circ$ (e.g. Platt and Behrmann, 1986). Due to this uncertainty, the method becomes unreliable in high-strain samples ($R_{XZ} > 10$–15) with small β ($<5^\circ$) where the obtained W_m spreads out over a wide range of possible values (Grasemann et al., 1999).

Both aforementioned methods employ data collected on the XZ-plane of finite strain and, therefore, they are not strictly valid for non-plane strain deformation. However, Tikoff and Fossen (1995) investigated the effect of the third stretching direction (Y-axis) on vorticity number estimates and demonstrated that the two-dimensional vorticity analysis can overestimate the actual, three-dimensional vorticity number by only a small amount (<0.05). In practice, this effect is very minor compared with the error in W_m values arising as a consequence of the uncertainty in assigning input data (i.e. β-angle) of these methods.

3. Strain-ratio and oblique-grain-shape fabric

Experimental studies (e.g. Herwegh and Handy, 1998) have shown that the maximum observed angle δ between the passive (S_B) and active (S_A) grain shape foliation is primarily related to both the degree of non-coaxiality and the shape of the strain ellipse just prior to the end of deformation. Based on this finding as well as on the aforementioned critical assumption that the grain shape foliation S_B may provide information about the extensional ISA, I shall

use a series of simple angular relationships in real and Mohr-circle space to express the angle δ as a function of R_{XZ} and W_n. The major elements of the Mohr-circle are illustrated in Fig. 2 (see Means, 1983; Passchier, 1988; Passchier and Urai, 1988; Wallis, 1992; Simpson and De Paor, 1993; Coelho and Passchier, 2008 for details).

For two-dimensional flow, the relationship between ISA and flow apophyses is given by $\theta = 90^\circ - 2\eta$ (e.g. Weijermars, 1991; Tikoff and Fossen, 1995) or:

$$90^\circ - \theta = 2(\delta + \beta) \tag{4}$$

since, as mentioned above, $\eta = \delta + \beta$ (Fig. 1a).

Also, in Mohr-circle space (e.g. right-triangle CEF in Fig. 2),

$$90^\circ - \theta = \alpha + \beta \tag{5}$$

substituting Eq. (5) into Eq. (4) and taking into account that $\varphi = \alpha - \beta$ (Fig. 2; Passchier, 1988; Wallis, 1992), it is demonstrated that:

$$2\delta = \varphi \tag{6}$$

note that φ defines the rotation of the line in the undeformed state that is now parallel to the largest principal strain axis (Fig. 2: inset; Passchier, 1988). Then, substituting the above relation (Eq. (6)) into Eq. (3), we can obtain the following equation:

$$W_n = \sin(2\delta)\frac{R_{XZ}+1}{R_{XZ}-1} \tag{7}$$

which shows that W_n is related to R_{XZ} and δ. Eq. (7) can be easily solved for δ and the result can be plotted for different W_n values:

$$\delta = \frac{1}{2}\sin^{-1}\left(W_n\frac{R_{XZ}-1}{R_{XZ}+1}\right) \tag{8}$$

this plot (R_{XZ} versus δ) is illustrated in the synthetic diagram of Fig. 3, which also includes an R_{XZ} versus β plot (Tikoff and Fossen, 1995; Grasemann et al., 1999) for comparison. This diagram indicates that during progressive steady-state deformation the angle δ attains a high value at low strain ($\sim R_{XZ} < 4$) and then is subjected to small changes. This observation appears to be in accordance with the experimental work of Herwegh and Handy (1998) who have argued that the oblique-grain-shape fabric forms early during non-coaxial shear attaining a stable orientation at low imposed shear strain ($\gamma < 1.5$). Plot of R_{XZ} versus δ also indicates that the W_n curves get broader spaced for increasing strain values (Fig. 3). This implies that, in contrast to the R_{XZ}/β-method, estimates of Eq. (7) are relatively insensitive to small changes in the values of R_{XZ} and δ. Based on these findings, it is suggested that Eq. (7) represents another potential technique (referred to hereinafter as R_{XZ}/δ-method) for extracting W_n from naturally deformed quartzites. The method describes instantaneous deformation and, therefore, does not require the assumption of steady-state deformation. However, it assumes monoclinic symmetry and theoretically is only valid for plane strain deformation conditions. This is because the orientation of ISA does not define a unique vorticity number for general 3D strain (Tikoff and Fossen, 1995). However, as mentioned above, the maximum expected error caused by assuming plane strain is only 0.05.

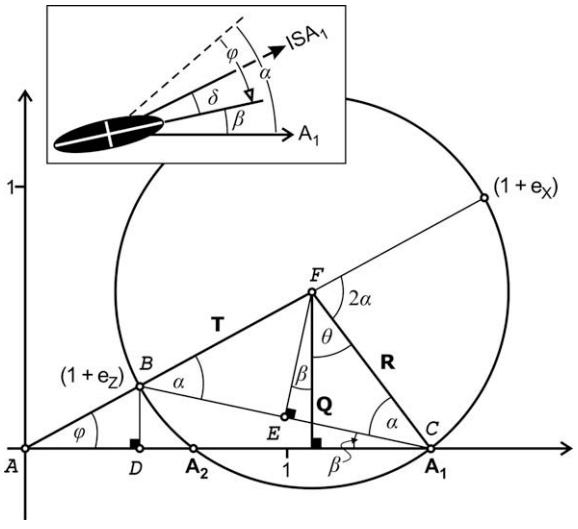

Fig. 2. Mohr-circle for the position gradient tensor representing finite deformation in stretch space (modified after Passchier, 1988; Vissers, 1989; Wallis, 1992). The distance (T) of the centre of the circle from the origin and the radius (R) of the circle are defined by the finite strain-ratio R_{XZ} [$=(1+e_X)/(1+e_Z)$]. The distance of the circle from the horizontal axis (Q) is a function of both the R_{XZ} and W_m. The angle φ defines the rotation of the line in the undeformed state that is now parallel to the principal strain axis X, while α is the original angle of this line with the A_1. θ defines the acute angle between the flow apophyses. The inset shows the parameters in real space.

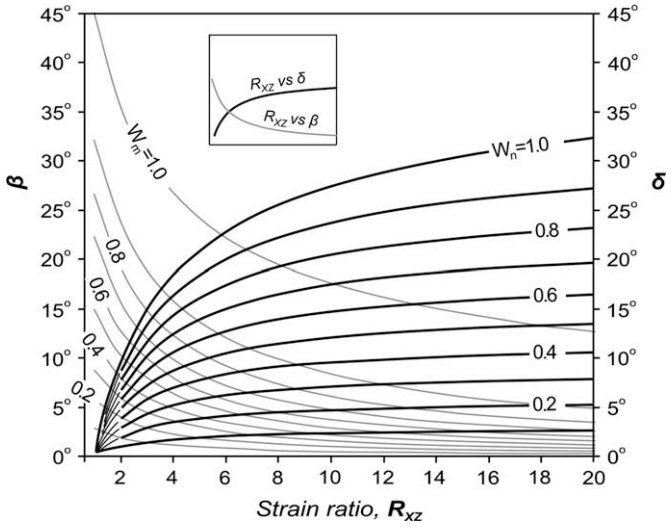

Fig. 3. Synthetic diagram showing plots of the finite strain-ratio R_{XZ} versus β (after Tikoff and Fossen, 1995; Grasemann et al., 1999) and R_{XZ} versus δ. See text for details.

4. Additions to previously proposed methods

From the study of the Mohr-circle in stretch space the following equation was also derived (Appendix A; Eq. (A4)):

$$R_{XZ}\tan^2\beta + R_{XZ}\tan\beta\tan\theta + \tan\beta\tan\theta = 1 \tag{9}$$

which can be solved for θ and, therefore W_m can be related to R_{XZ} and β:

$$W_m = \cos\theta = \cos\left[\tan^{-1}\left(\frac{1 - R_{XZ}\tan^2\beta}{(1+R_{XZ})\tan\beta}\right)\right] \tag{10}$$

Eq. (10) is an alternative equation for the R_{XZ}/β-method. It gives the same W_m values as the equations (Eqs. (3) and (4)) proposed by Wallis (1995; his eqs. 8 and 9), but it is probably a more useful expression since it is directly comparable with other vorticity equations that are also expressed in the form $W_m = \cos(\arctan(fx))$ (e.g. Bobyarchick, 1986; Tikoff and Fossen, 1993). Note also that by applying Eq. (10) for $R_{XZ} = 1$ the relation $\theta = 90^\circ - 2\beta$ is obtained, which leads to the predictable conclusion that the largest principal strain axis rotates from the position of ISA_1 at the infinitesimally small strain towards A_1 (e.g. Passchier, 1997).

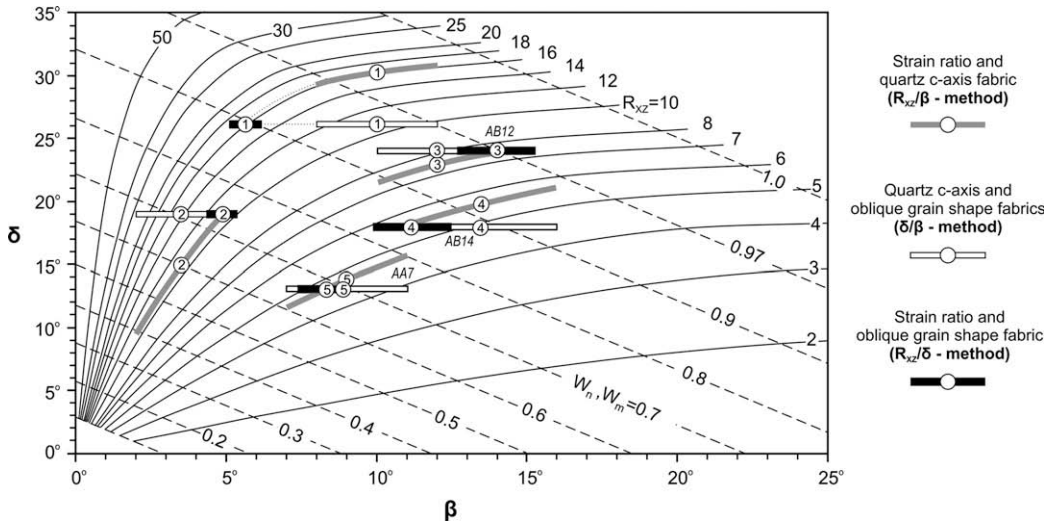

Fig. 4. Suggested nomogram for estimating W_m (or W_n) and R_{XZ} in naturally deformed quartzites and an application to five representative samples. Two of them (1, 2) are from the Elba Quartzite in Raft River Mountains (Sullivan, 2008; his sample RR21, RR08 and table 2). The other three cases (3–5) are from the Phyllite–Quartzite unit of the External Hellenides and correspond to samples AB12, AB14 and AA7, respectively. Data for these samples are given in Appendix B. Circles indicate estimates obtained using the best assigned input data. Error bars were constructed using uncertainty in the estimations of the β-angle as well as error in R_{XZ} values.

Eq. (9) can be also solved for R_{XZ}. Therefore, if deformation is steady-state and, both β and δ are known, an estimate of the R_{XZ} can be obtained using the relation:

$$R_{XZ} = \frac{1 - \tan\theta \cdot \tan\beta}{\tan^2\beta + \tan\theta \cdot \tan\beta} \qquad (11)$$

where: $\tan\theta = \cot[2(\beta+\delta)]$ or $= \sqrt{1 - W_m^2}/W_m$ (Passchier, 1988).

Note that a different equation, which is derived by the standard solution to a quadratic equation, has been proposed by Wallis (1995; his eq. 13) for relating W_m, β and R_{XZ}. R_{XZ} values obtained by Eq. (11) coincide with one of two possible solutions of Wallis's (1995) equation.

5. A vorticity nomogram

By using both Eq. (8) and the solution of Eq. (9) for β (Appendix A; Eq. (A5)), it is possibly to construct a nomogram that incorporates all the parameters (β, δ, R_{XZ} and W_n/W_m) involved in the three vorticity analysis methods. As illustrated in Fig. 4, this nomogram is a planar graph of β versus δ for different W_n (or W_m) and R_{XZ} values. The advantages of such nomographical approach are multi-fold: (1) it instantly provides the vorticity number for all methods; (2) it allows to check, for all methods, the sensitivity of estimated vorticity numbers values in changes of input parameters (β, δ, R_{XZ}); (3) it provides a rapid means of evaluating the consistency of values estimated by the various methods; (4) it permits the presentation of uncertainties in vorticity number estimates as error bars; (5) it enables the rapid evaluation of mean strain level for a suite of samples, where only β- and δ-angle data are available.

6. Application to natural examples

Quartz-rich tectonites of the Phyllite–Quartzite (PQ) unit of the Hellenides (Fig. 5) provide an opportunity to demonstrate the utility of the R_{XZ}/δ-method, test the descriptive ability of the nomogram, and explore whether or not Eq. (11) may be used as an indirect means for estimating R_{XZ} values. The PQ unit is considered to be a mid-crustal extruding shear zone, which is bounded by a west-directed ductile thrust fault at the base (basal thrust) and an east-directed fault with apparent normal shear sense at the top (Fig. 5a: A–A′; e.g. Xypolias and Doutsos, 2000). This westward extrusion process is associated with the main phase of ductile deformation (here D_A) in the PQ unit, which produced a penetrative foliation (S_A) and a stretching lineation (Fig. 5b) (Zulauf et al., 2002; Xypolias et al., 2008 and references therein). Previous microstructural, petrofabric and finite strain studies, demonstrated that D_A-deformation occurred under approximately plane strain conditions

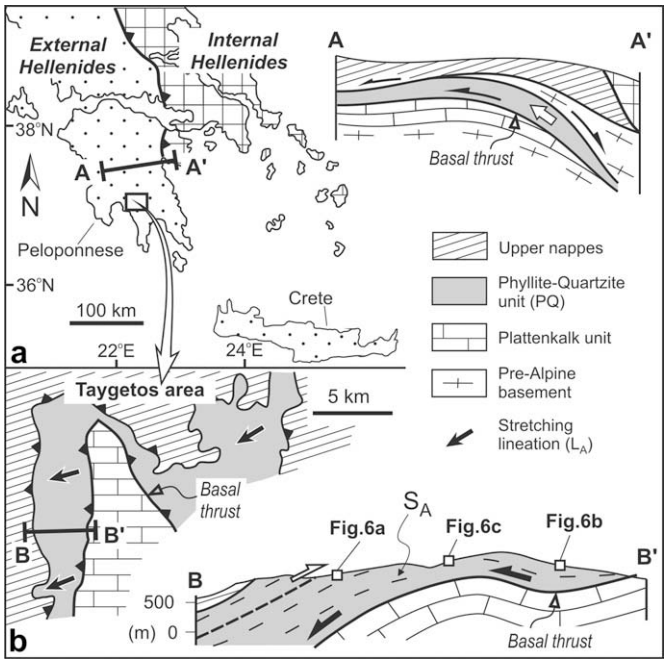

Fig. 5. (a) Generalized map of the Hellenides in southwestern Greece and schematic crustal-scale profile (A–A′) showing the ductile exhumation of the Phyllite–Quartzite unit under a solid state extrusion mechanism (after Xypolias and Doutsos, 2000). (b) Geological map of the Taygetos area and cross-section (B–B′) within the Phyllite–Quartzite unit (modified after Xypolias and Kokkalas, 2006). Samples discussed here have been collected from this section at different distance above the basal thrust (Appendix B). Note that the observed flexure of the basal thrust was formed during a brittle phase of deformation which followed the west-directed extrusion the Phyllite–Quartzite unit.

and supported monoclinic flow (e.g. Xypolias and Koukouvelas, 2001; Zulauf et al., 2002). This application focuses on an indicative section of the PQ unit in the Taygetos area (Fig. 5b). The prominent structures in this section are the basal thrust as well as a thin, foliation parallel zone of backward (eastward) shearing that was developed at the upper structural levels of the unit during the late-stages of D_A-deformation (Fig. 5b; B–B′). Quartz *c*-axis-fabric and finite strain data for a suite of samples, which are located at different distance above the basal thrust, are available from a recent study in this section (Xypolias and Kokkalas, 2006; β and R_{XZ} values in Appendix B). These samples are strongly foliated and lineated, and composed mainly of quartz and lesser amount of phyllosilicate minerals (Fig. 6a). Quartz aggregates show evidence of dynamic recrystallization accommodated by both subgrain rotation and low-temperature grain-boundary migration (regime II of Hirth and Tullis, 1992). Maximum deformation temperature has been evaluated at about 450 °C (Xypolias and Kokkalas, 2006). For the purpose of this study, the *XZ* thin sections of these samples were re-examined and the original data set was supplemented with measurements of δ angle between S_A and S_B foliation (Fig. 6a–c; Appendix B). S_B foliation was identified in 14 out of 29 analyzed samples. The estimated δ values range between 9 and 24°, but appear to be fairly constant within individual samples.

Finite strain ratio R_{XZ} in these samples generally varies from 3.5 to 8.0 (Appendix B). Note that these R_{XZ} values were calculated from the shape of plastically elongated, slightly recrystallized quartz grains lying in the plane of main foliation (S_A) while analyses of shape data were performed using algebraic and geometry Rf/φ methods (e.g. Xypolias et al., 2007). Where possibly, the R_{XZ} values were also estimated using Eq. (11) for β and δ values. Fig. 7 is a comparative chart, for 11 samples, showing differences between R_{XZ} estimates obtained by using Eq. (11) and R_{XZ} values that were independently calculated from quartz grain shapes. The comparison revealed that the percentage error within individual samples can range from 2 to 35%. However, for the whole suite of samples, the obtained and the calculated R_{XZ} values have the same average values (Fig. 7). This example may imply that Eq. (11) could be used to evaluate mean strain levels in dynamically recrystallized quartzite samples where suitable strain markers are not observed.

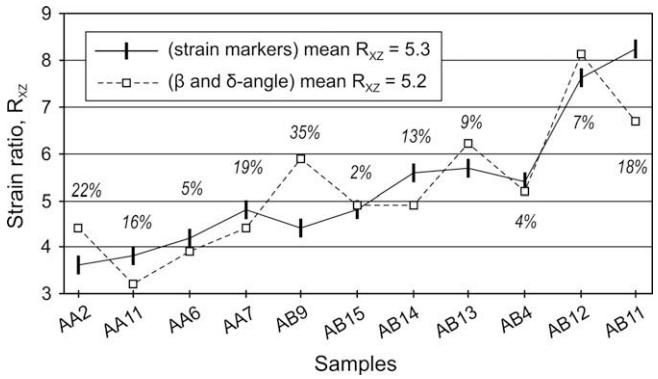

Fig. 7. Comparative charts showing differences between R_{XZ} estimates obtained by using Eq. (11) for β and δ values, and R_{XZ} values that were independently calculated by using common elliptical strain markers (e.g. elongated quartz grains) lying in the plane of foliation. Percentage error in each case is also shown. Raw data for all samples are given in Appendix B. Chart constructed using the best assigned β and δ values.

Data from five representative samples were plotted on the nomogram to compare results of R_{XZ}/δ with those of two other vorticity methods (Fig. 4). Three of them are derived from the PQ unit (Fig. 4; cases 3–5) while the other two from the high-strain rocks of the Elba Quartzite in Raft River Mountains (Fig. 4; cases 1,

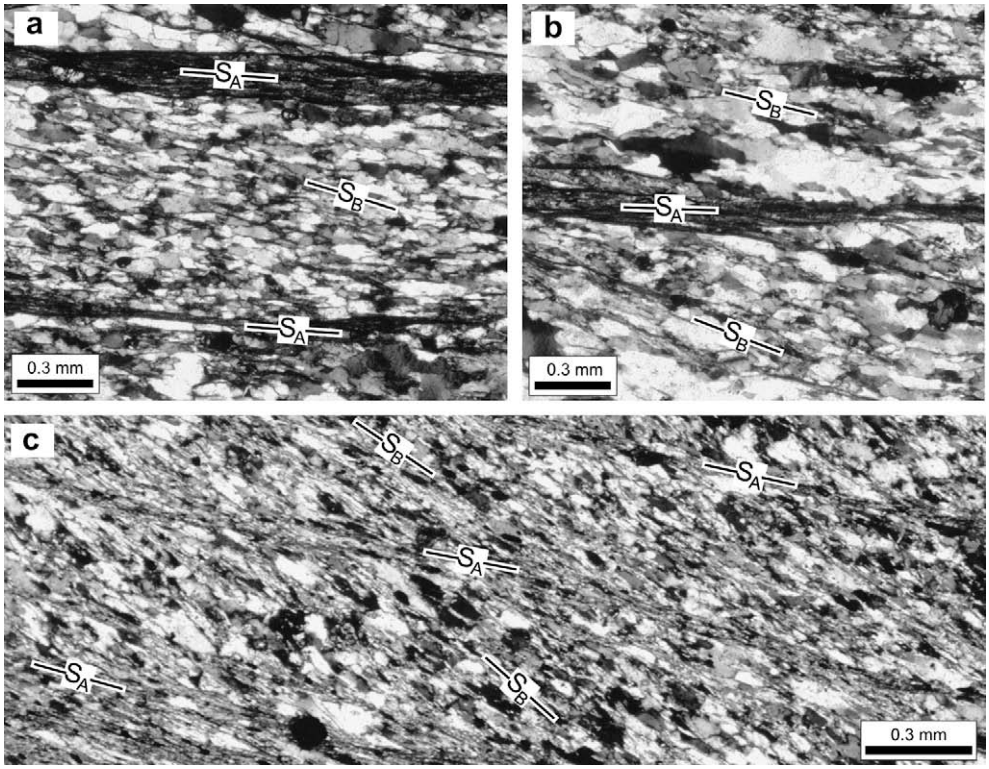

Fig. 6. Micrographs (crossed nicols) of samples from the Phyllite–Quartzite unit in Taygetos area showing angular relationships between the main (S_A) and the oblique (S_B) foliation. The S_A is mainly defined by the alignment of micaceous films and flattened quartz grains while the S_B by the shape preferred orientation of dynamically recrystallized quartz grains. The samples are located at structural distances (a) 720 m (sample AA7), (b) 390 m (sample AB14) and (c) 240 m (sample AB5) above the basal thrust. For location of samples see Fig. 5b. All micrographs are from thin sections cut perpendicular to S_A and parallel to stretching lineation; view towards the north; top-to-the west sense of shear.

2). The later samples were used in order to cover a wide spectrum of possibly strain values. Data for these samples are derived by a recent vorticity study (Sullivan, 2008; his sample RR21, RR08) in Elba Quartzite, where both the R_{XZ}/β and δ/β-methods have been applied. Based on the vorticity analysis results illustrated in the nomogram (Fig. 4), the following observations may be drawn:

(1) The range of uncertainty in W_n values estimated by the R_{XZ}/δ-method is smaller than this recorded by each of the other two methods. This holds true even if it is assumed that the determination of δ value includes an uncertainty of around 5°.
(2) Results like this of case example 5 (Fig. 4), where all methods give nearly similar values, seems to be the exception than the norm. Wallis (1995) interpreted the discrepancy between the results of R_{XZ}/β- and δ/β-method to reflect change of flow regime during progressive deformation. By analogy, this observation could also be interpreted as indicative of non-steady-state deformation.
(3) The δ/β-method gives estimates between those obtained by the R_{XZ}/β- and R_{XZ}/δ-method. This observation can be explained if it is considered that quartz *c*-axis-fabric may retain information for a relatively long part of the deformation history (Law, 1986; Hippertt and Borba, 1992; Wallis, 1995) and survives late-stage changes in the kinetic boundary conditions (e.g. Herwegh and Handy, 1998). Therefore, it can be assumed that angle β may not be an instantaneous sensitive feature. In contrast, the oblique-grain-shape fabric, and therefore the angle δ, is by definition prone to late-stage resetting. As a result, it seems that the three methods may have different strain memory sampling different parts of deformation history. It is possibly that the R_{XZ}/β-method has the longest strain memory while the R_{XZ}/δ-method provides information about the last increment of plastic deformation. The δ/β-method records an intermediate part of this deformation history.
(4) The estimated W_n values using R_{XZ}/δ-method are either lower or greater than those obtained by both other methods. This fact may indicate the trend of change in W_n during progressive deformation.

6.1. Test at regional scale

To test the tectonic significance of the above-mentioned observations as well as the utility of R_{XZ}/δ-method, the spatial variation of the vorticity number within the PQ unit was explored. Previous study (Xypolias and Kokkalas, 2006) in Taygetos section described a vorticity profile within the PQ unit using W_m values estimated by the R_{XZ}/β – as well as by the rigid porphyroclasts method (Passchier, 1987) (Fig. 8a). The general trend observed by 'averaging' the results of these methods is that the W_m value approaches 1 close to the basal thrust and decreases upwards reaching a value of ~0.7 at the top of the PQ unit (Fig. 8b). This trend is partly modified if we re-examined the spatial variation on the basis of R_{XZ}/δ-method estimates obtained incorporating R_{XZ} with δ values data from 14 analyzed samples (Fig. 8a; Appendix B). In this case, vorticity profile indicates a significant decrease in W_n value at the middle of the unit, below the zone of backward shearing (Fig. 5: B–B′), and an increase in W_n value above this zone (Fig. 8b). A corresponding but ill-defined variation in W_m is observed in the vorticity profile constructed using the results of the R_{XZ}/β-method only (Fig. 8b). Therefore, adopting the aforementioned hypothesis, that two methods record different parts of deformation history, it can be suggested that domains above and below the zone of local backward shearing were deforming with an increasing simple and pure shear component, respectively. This possibly created a progressively increasing problem of strain

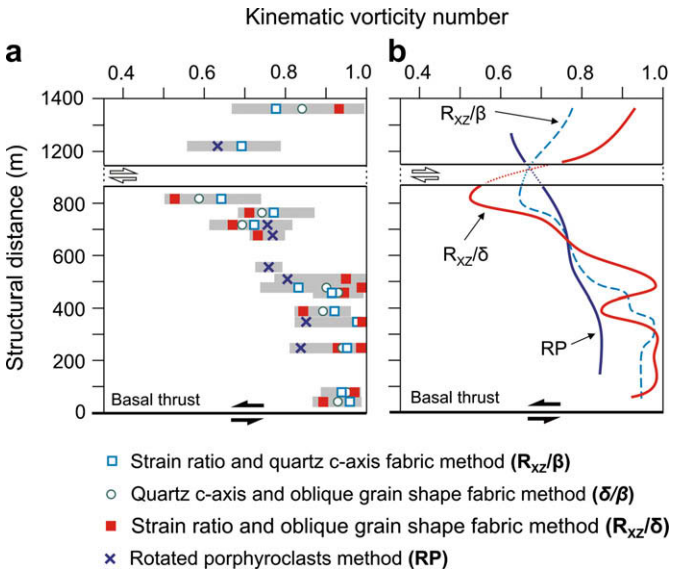

Fig. 8. Graphs (vorticity profiles) illustrating the vertical spatial variation in W_n/W_m values within the Phyllite–Quartzite unit in Taygetos areas. Length of grey scale bars (a) reflects the uncertainty in the calculation of kinematic vorticity number arising as a consequence of the difficulty in accurately assigning input data from all applied vorticity methods. Vorticity profiles in (b) were constructed using the best estimated W_n (or W_m) values obtained by the R_{XZ}/β, R_{XZ}/δ and rigid porphyroclast vorticity methods. Vorticity estimates obtained by the R_{XZ}/β and rigid porphyroclasts methods after Xypolias and Kokkalas (2006). Raw data are given in Appendix B.

compatibility which may explain why the zone of backward shearing formed during the last stage of ductile deformation. Moreover, it is worth noting that vorticity profile obtained by the W_m estimates of rigid porphyroclasts method appear to remain unaffected by any local late-stage change in the flow regime (Fig. 8b). This profile also seems to 'average' profiles obtained by quartz based methods. So, it can be concluded that the analysis of rigid porphyroclasts gives results close to the real mean vorticity of flow.

The above natural examples indicate that the R_{XZ}/δ-method is a valuable means for extracting vorticity number from quartz-rich tectonites. It can also provide information about deformation history when compared with other quartz based methods. However, the application of these methods is limited by a number of necessary assumptions. The idealized model of monoclinic flow is one of them, provided that more complex systems (i.e. triclinic flow) can also produce shape and crystal fabrics as those used in these methods. At present, it remains unclear (e.g. Iacopini et al., 2007).

7. Conclusions

The incorporation of strain data measured in the *XZ*-plane of finite strain (R_{XZ}) with values of the angle δ between the oblique-grain-shape fabric and the main foliation can serve as an additional method for estimating vorticity number from naturally deformed quartzites. This method potentially records the influence of the flow immediately prior to fossilization of the fabric. Natural examples also showed that the new method is able to record late-stage changes in the flow regime that are slightly or not detectable by vorticity methods which incorporates data for the geometry of quartz *c*-axis-fabrics with R_{XZ} or angle δ values. However, due to uncertainties inherent in evaluating input parameters of all methods, it is strongly recommended that vorticity analysis in naturally deformed quartzites should be performed by applying as many methods as possible in a given

sample. The use of a newly proposed nomogram that incorporates all the parameters involved in the quartz based vorticity method can facilitate this task.

Acknowledgments

Constructive reviews by Simon Wallis and Chuck Bailey substantially improved the manuscript and are gratefully acknowledged.

Appendix A

Using the trigonometric ratio (in the Mohr-circle space) of the angles φ and β in the right-triangles DCB and DAB, respectively, we have that the length BD is equal to (Fig. 2):

$$\mathrm{BC}\sin\beta = (T-R)\sin\varphi \tag{A1}$$

Moreover, from the right-triangle EFC (Fig. 2) and the relation $\varphi=\alpha-\beta$ (Wallis, 1992), we get these:

$$\mathrm{BC} = \sin(\beta+\theta)2R \tag{A2}$$

$$\varphi = 90^\circ-(\beta+\theta)-\beta \tag{A3}$$

substitution of Eq. (A2) and Eq. (A3) into Eq. (A1) yields:

$$2R\sin(\beta+\theta)\sin\beta = (T-R)\sin\left[(90^o-(\beta+\theta))-\beta\right]$$

which is simplified by using the angle difference identity for sine as follows:

$$2R\sin(\beta+\theta)\sin\beta = (T-R)\cos(\beta+\theta)\cos\beta - (T-R)\sin(\beta+\theta)\sin\beta$$

Rearranging, and then collecting terms in $\sin(\beta+\theta)\sin\beta$, these become:

$$(T+R)\sin(\beta+\theta)\sin\beta = (T-R)\cos(\beta+\theta)\cos\beta$$

Dividing left-hand by right-hand side and taking into account that $[(\mathrm{T}+\mathrm{R})/(\mathrm{T}-\mathrm{R})]=R_{XZ}$ (Passchier, 1988) we get:

$$R_{XZ}\tan(\beta+\theta)\tan\beta = 1$$

Finally, by applying the angle sum identity for tangent, and then simplifying we have:

$$R_{XZ}\tan^2\beta + R_{XZ}\tan\beta\tan\theta + \tan\beta\tan\theta = 1 \tag{A4}$$

Eq. (A4) can be easily solved for θ (Eq. (10)), and R_{XZ} (Eq. (11)). Collecting terms in $\tan\beta$ and rearranging, the following equation is obtained:

$$R_{XZ}\tan^2\beta + ((R_{XZ}+1)\tan\theta)\tan\beta - 1 = 0$$

which can be solved for β by using the standard solution to a quadratic equation:

$$\beta = \tan^{-1}\left|\frac{-(R_{XZ}+1)\tan\theta \pm \left[(R_{XZ}+1)^2\tan^2\theta + 4R_{XZ}\right]^{1/2}}{2R_{XZ}}\right| \tag{A5}$$

where $\tan\theta = \sqrt{1-W_m^2}/W_m$ (Passchier, 1988).

Appendix B

Sample	D^* (m)	β^* (°)	δ (°)	$R_{XZ}^* \pm$ error
AA2	1380	10–15	16	3.6 ± 0.3
AA10	1230	8–13	–	3.5 ± 0.4
AA11	820	7–11	9	3.8 ± 0.4
AA6	770	9–13	13	4.2 ± 0.4
AA7	720	7–11	13	4.8 ± 0.4
AA5	690	–	14	4.6 ± 0.3
AB17	500	–	21	5.8 ± 0.6
AB9	480	10–15	20	4.4 ± 0.3
AB15	470	13–17	19	4.8 ± 0.5
AB14	390	11–16	18	5.6 ± 0.4
AB13	350	18–22	23	5.7 ± 0.6
AB4	250	13–18	20	5.4 ± 0.6
AB5	240	–	24	6.7 ± 0.4
AB12	80	10–14	24	7.6 ± 0.4
AB11	60	11–15	22	8.2 ± 0.6

D: structural distance from the basal thrust.
*After Xypolias and Kokkalas (2006; their fig. 2 and table 1).

References

Bailey, C.M., Eyster, E.L., 2003. General shear deformation in the Pinaleno Mountains metamorphic core complex, Arizona. Journal of Structural Geology 25, 1883–1893.

Bailey, C.M., Francis, B.E., Fahrney, E.E., 2004. Strain and vorticity analysis of transpressional high-strain zones from the Virginia Piedmont, USA. In: Aslop, G.I., Holdsworth, R.E., McCaffrey, K.J.H., Hand, M. (Eds.), Flow Processes in Faults and Shear Zones. Geological Society, Special Publications, vol. 224, pp. 249–264.

Bobyarchick, A., 1986. The eigenvalues of steady state flow in Mohr space. Tectonophysics 122, 35–51.

Bouchez, J.L., Duval, P., 1982. The fabric of polycrystalline ice deformed in simple shear: experiments in torsion, natural deformation and geometrical interpretation. Textures and Microstructures 5, 171–190.

Coelho, S., Passchier, C., 2008. Mohr-cyclides, a 3D representation of geological tensors: the examples of stress and flow. Journal of Structural Geology 30 (5), 580–601.

Forte, A.M., Bailey, C.M., 2007. Testing the utility of the porphyroclast hyperbolic distribution method of kinematic vorticity analysis. Journal of Structural Geology 29, 983–1001.

Grasemann, B., Fritz, H., Vannay, J.C., 1999. Quantitative kinematic flow analysis from the Main Central Thrust Zone (NW-Himalaya, India): implications for a decelerating strain path and the extrusion of orogenic wedges. Journal of Structural Geology 21, 837–853.

Heilbronner, R., Tullis, J., 2006. Evolution of *c*-axis pole figures and grain size during dynamic recrystallization: results from experimentally sheared quartzite. Journal of Geophysical Research 111, B10202, doi:10.1029/2005JB004194.

Herwegh, M., Handy, M.R., 1996. The evolution of high temperature mylonitic microfabrics: evidence for simple shearing of a quartz analogue (norcamphor). Journal of Structural Geology 18, 689–710.

Herwegh, M., Handy, M.R., 1998. The origin of shape preferred orientations in mylonite: inferences from in-situ experiments on polycrystalline norcamphor. Journal of Structural Geology 20, 681–694.

Herwegh, M., Handy, M.R., Heilbronner, R., 1997. Temperature- and strain rate-dependent microfabric evolution in monomineralic mylonite: evidence from in-situ deformation of norcamphor. Tectonophysics 280, 83–106.

Hippertt, J.F.M., Borba, R.P., 1992. Quartz *c*-axis fabric differences between porphyroclasts and recrystallized grains: discussion. Journal of Structural Geology 14, 627–630.

Hirth, G., Tullis, J., 1992. Dislocation creep regimes in quartz aggregates. Journal of Structural Geology 14, 145–159.

Iacopini, D., Carosi, R., Montomoli, C., Passchier, C.W., 2008. Strain analysis and vorticity of flow in the Northern Sardinian Variscan Belt: recognition of a partitioned oblique deformation event. Tectonophysics 446, 77–96.

Iacopini, D., Passchier, C.W., Koehn, D., Carosi, R., 2007. Fabric attractors in general triclinic flow systems and their application to high strain shear zones: a dynamical system approach. Journal of Structural Geology 29, 298–317.

Jessup, M.J., Law, R.D., Frassi, C., 2007. The rigid grain net (RGN): an alternative method for estimating mean kinematic vorticity number (W_m). Journal of Structural Geology 29, 411–421.

Jessup, M.J., Law, R.D., Searle, M.P., Hubbard, M.S., 2006. Structural evolution and vorticity of flow during extrusion and exhumation of the Greater Himalayan Slab, Mount Everest Massif, Tibet/Nepal: implications for orogen-scale flow partitioning. In: Law, R.D., Searle, M.P., Godin, L. (Eds.), Channel Flow, Extrusion, and Exhumation in Continental Collision Zones. Geological Society, London, Special Publications, vol. 268, pp. 379–414.

Jiang, D., Williams, P.F., 1998. High-strain zones: a unified model. Journal of Structural Geology 20, 1105–1120.

Law, R.D., 1986. Relationships between strain and quartz crystallographic fabrics in the Roche Maurice quartzites of Plougastel, western Brittany. Journal of Structural Geology 8, 493–515.
Law, R.D., 1990. Crystallographic fabrics: a selective review of their applications to research in structural geology. In: Knipe, R.J., Rutter, E.H. (Eds.), Deformation Mechanisms, Rheology and Tectonics. Geological Society, London, Special Publications, vol. 54, pp. 335–352.
Law, R.D., Knipe, R.J., Dayan, H., 1984. Strain-path partitioning within thrust sheets: microstructural and petrofabric evidence from the Moine thrust zone at Loch Eriboll, northwest Scotland. Journal of Structural Geology 6, 477–497.
Law, R.D., Searle, M.P., Simpson, R.L., 2004. Strain, deformation temperatures and vorticity of flow at the top of the Greater Himalayan Slab, Everest Massif, Tibet. Journal of the Geological Society, London 161, 305–320.
Lister, G.S., Hobbs, B.E., 1980. The simulation of fabric development during plastic deformation and its application to quartzite: the influence of deformation history. Journal of Structural Geology 2, 355–370.
Means, W.D., 1981. The concept of steady-state foliation. Tectonophysics 78, 179–199.
Means, W.D., 1983. Application of the Mohr-circle construction to problems of inhomogeneous deformation. Journal of Structural Geology 5, 279–286.
Means, W.D., Hobbs, B.E., Lister, G.S., Williams, P.F., 1980. Vorticity and non-coaxiality in progressive deformations. Journal of Structural Geology 2, 371–378.
Passchier, C.W., 1987. Stable positions of rigid objects in non-coaxial flow: a study in vorticity analysis. Journal of Structural Geology 9, 679–690.
Passchier, C.W., 1988. The use of Mohr circles to describe non-coaxial progressive deformation. Tectonophysics 149, 323–338.
Passchier, C.W., 1997. The fabric attractor. Journal of Structural Geology 19, 113–127.
Passchier, C.W., Trouw, R.A.J., 2005. Microtectonics, second ed. Springer Verlag, Berlin–Heidelberg–New York.
Passchier, C.W., Urai, J.L., 1988. Vorticity and strain analysis using Mohr diagrams. Journal of Structural Geology 10, 755–763.
Platt, J.P., Behrmann, J.H., 1986. Structures and fabrics in a crustal scale shear zone, Betic Cordilleras, S.E. Spain. Journal of Structural Geology 8, 15–34.
Ree, J.H., 1991. An experimental steady-state foliation. Journal of Structural Geology 13, 1001–1011.
Simpson, C., De Paor, D.G., 1993. Strain and kinematic analysis in general shear zones. Journal of Structural Geology 15, 1–20.
Srivastava, H.B., Hudleston, P., Earley, D., 1995. Strain and volume loss in a ductile shear zone. Journal of Structural Geology 17, 1217–1231.
Sullivan, W.A., 2008. Significance of transport-parallel strain variations in part of the Raft River shear zone, Raft River Mountains, Utah, USA. Journal of Structural Geology 30, 138–158.
Sullivan, W.A., Law, R.D., 2007. Deformation path partitioning within the transpressional White Mountain shear zone, California and Nevada. Journal of Structural Geology 29, 583–598.
Tikoff, B., Fossen, H., 1993. Simultaneous pure shear and simple shear: the unifying deformation matrix. Tectonophysics 217, 267–283.
Tikoff, B., Fossen, H., 1995. The limitations of three-dimensional kinematic vorticity analysis. Journal of Structural Geology 17, 1771–1784.
Vissers, R.L.M., 1989. Asymmetric quartz *c*-axis fabrics and flow vorticity: a study using rotated garnets. Journal of Structural Geology 11, 231–244.
Wallis, S.R., 1992. Vorticity analysis in a metachert from the Sanbagawa Belt, SW Japan. Journal of Structural Geology 14, 271–280.
Wallis, S.R., 1995. Vorticity analysis and recognition of ductile extension in the Sanbagawa belt, SW Japan. Journal of Structural Geology 17, 1077–1093.
Weijermars, R., 1991. The role of stress in ductile deformation. Journal of Structural Geology 13, 1061–1078.
Xypolias, P., Chatzaras, V., Koukouvelas, I.K., 2007. Strain gradients in zones of ductile thrusting: insights from the External Hellenides. Journal of Structural Geology 29, 1522–1537.
Xypolias, P., Doutsos, T., 2000. Kinematics of rock flow in a crustal-scale shear zone: implication for the orogenic evolution of the southwestern Hellenides. Geological Magazine 137, 81–96.
Xypolias, P., Kokkalas, S., 2006. Heterogeneous ductile deformation along a mid-crustal extruding shear zone: an example from the External Hellenides (Greece). In: Law, R.D., Searle, M.P., Godin, L. (Eds.), Channel flow, Extrusion, and Exhumation in Continental Collision Zones. Geological Society, London, Special Publications, vol. 268, pp. 497–516.
Xypolias, P., Koukouvelas, I.K., 2001. Kinematic vorticity and strain rate patterns associated with ductile extrusion in the Chelmos Shear Zone (External Hellenides, Greece). Tectonophysics 338, 59–77.
Xypolias, P., Koukouvelas, I.K., Zulauf, G., 2008. Cenozoic tectonic evolution of northeastern Apulia: insights from a key study area in the Hellenides (Kythira, Greece). In: Xypolias, P., Zulauf, G. (Eds.), New Results and Concepts on the Regional Geology of the Eastern Mediterranean. Zeitschrift der Deutschen Gesellschaft für Geowissenschaften, 159, pp. 439–455.
Zulauf, G., Kowalczyk, G., Krahl, J., Petschick, R., Schwanz, S., 2002. The tectono-metamorphic evolution of high-pressure low-temperature metamorphic rocks of eastern Crete, Greece: constraints from microfabrics, strain, illite crystallinity and paleodifferential stress. Journal of Structural Geology 24, 1805–1828.